PHYSICAL REVIEW B

CONDENSED MATTER

THIRD SERIES, VOLUME 42, NUMBER 12 15 OCTOBER 1990-II

Angular distribution of Rh atoms desorbed from ion-bombarded Rh{100}: Effect of local environment

R. Maboudian, Z. Postawa,* M. El-Maazawi, B. J. Garrison, and N. Winograd

Department of Chemistry, The Pennsylvania State University, University Park, Pennsylvania 16802

(Received 14 May 1990)

Energy-resolved angular distributions of Rh atoms desorbed by 5 keV Ar-ion bombardment of the Rh{100} surface are measured with use of a multiphoton resonance ionization technique. The results are shown to be in a good agreement with molecular-dynamics simulations of the ion-impact event using the same interaction potential optimized previously to describe desorption from Rh{111}. In addition, by analyzing contour plots of the surface potential energy, the trend in the experimental results for Rh{100} and those previously published for Rh{111} are well explained. Based on this analysis, it is concluded that the peak in the polar-angle distribution of neutral particles desorbed from ion-bombarded single crystals is mainly determined by the relative positions of surface atoms which influence the trajectory of an exiting particle via channeling and blocking. Moreover, the anisotropy of the momentum imparted to the surface atoms in the last collision leads to an enhancement of ejection along certain crystallographic directions.

I. INTRODUCTION

It has been known for over three decades that the angular distributions of particles desorbed from ion-bombarded single crystals show characteristic anisotropies corresponding to preferred ejections along certain low-Miller-index crystallographic directions.[1] Despite much experimental and theoretical work since their first observation,[2] the underlying mechanism remains somewhat controversial.[1] From a theoretical point of view, two main models have been proposed. One is the so-called focusing collision theory[3] that assumes that the inherent crystalline order brings about a correlation between the successive collisions. This, in turn, leads to a preferential propagation of energy along close-packed rows of atoms and thus enhanced particle ejection in such directions. Second is the Lehmann-Sigmund mechanism, which employs the structure of the surface to explain the ejection pattern.[4] However, due to their neglect of the full three-dimensional structure of the crystal and their use of oversimplified assumptions, these models can only provide a qualitative account of the observed phenomena.[1] Computer simulations of the ion-impact event, on the other hand, overcome these limitations and can offer a detailed picture of the mechanisms leading to the angular anisotropies. This approach, in turn, falls into two groups.[1,5,6] One is the binary-collision approximation, where the particle trajectory is taken as a sequence of two-body collisions. The second involves molecular-dynamics (MD) calculations, where simultaneous interactions of atoms in the model crystal are taken into consideration. Although the computer simulations have shown great promise, the progress, until recently, has been somewhat hindered due to lack of detailed and reliable experimental measurements.

Many early experimental results, while exhibiting strong anisotropies, are characterized by poorly defined surfaces and lack of specificity in the data collection.[7] The data were taken with high background pressures and large fluences of incident ions. The surfaces were partly reacted and partly damaged. In addition, there was no mass or energy discrimination in measuring the angular distributions. However, recently, a novel multiphoton resonance ionization technique has been employed that circumvents these problems.[8] By using a position-sensitive detection scheme, energy and angular distributions of desorbed species may be measured simultaneously with low ion doses ($< 10^{13}$ ions/cm^2). This way, it is possible to make direct and detailed comparisons to the theoretical predictions. The results of such measurements on Rh{111} have already been presented[9] and compared successfully to the molecular-dynamics simulations of the desorption process.[10,11] Based on this comparison, it was concluded that the angular distribution of

Rh atoms ejected from ion-bombarded Rh{111} reflects the crystal structure of the near-surface region. This structural sensitivity was shown to be a consequence of the surface atoms, while desorbing, being channeled, and blocked in particular directions along the surface.[9–11]

Here, we report, using the same technique, the energy-resolved angular distributions of Rh atoms ejected from an ion-bombarded Rh{100} crystal. This surface is less densely packed, and hence the channeling and blocking mechanism is expected to be more effective. The results are shown to be well reproduced by the MD calculations of the ion-impact process. In addition, a comparison between the distributions from Rh{100} to the previously published results[9] on Rh{111} strongly suggests that there are at least two factors involved in determining the ejection pattern. One is the relative positions of the surface atoms which influence the trajectory of an exiting particle via channeling and blocking. The second is the anisotropy of the momentum transmitted to the surface atoms in the final collision leading to an enhanced ejection along certain crystallographic directions. Both factors intimately reflect the local structure of the surface near the region of the desorbing atom.

II. EXPERIMENT

The experimental arrangement is described in detail elsewhere.[8] Briefly, as is shown in Fig. 1, it consists of an ultrahigh-vacuum (UHV) chamber (2×10^{-10} Torr base pressure) equipped for low-energy electron diffraction (LEED) and Auger spectroscopy, an ion source for ion bombardment of the sample, a tunable neodymium-doped yttrium aluminum garnet (Nd:YAG) pumped dye laser with a frequency doubler to resonantly ionize the desorbed neutrals, a position-sensitive microchannel-plate (MCP) detector with a phosphor screen in the back of it, and an image-processing system which includes a charge-coupled-device (CCD) camera interfaced to a Digital Equipment Corporation micro-VAX station II computer via a real-time frame grabber.

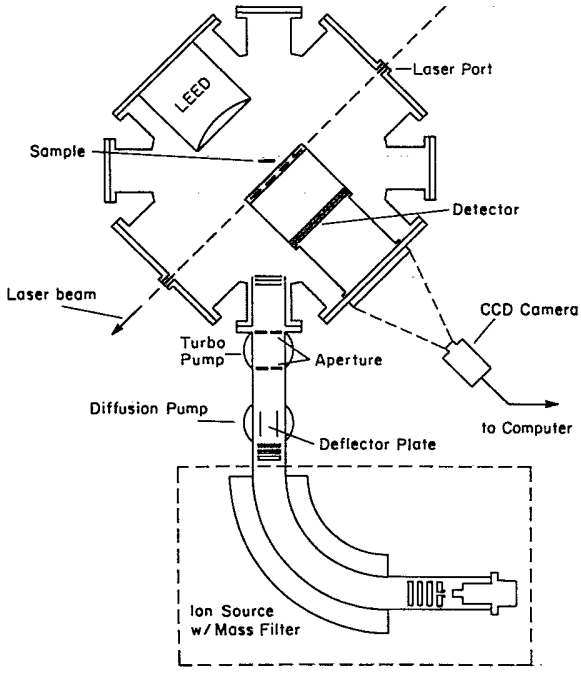

FIG. 1. Top view of the experimental setup used to measure energy- and angle-resolved distributions of neutral atoms desorbed from ion-bombarded surfaces.

The Rh sample is an optically polished single crystal of 99.99% purity oriented to within $\pm0.5°$ of the (100) face. The cleaning procedure involves many cycles of ion bombardment (5-keV Ar^+, 4 $\mu A/cm^2$, 20 min) and annealing (950 K, 20 min), followed by annealing in oxygen (10^{-7} Torr, 950 K, 20 min) and hydrogen (10^{-7} Torr, 600 K, 20 min).[12–14] A final flash to 1400 K results in a sharp (1×1) LEED pattern with low background.

The experiment proceeds as follows. A pulse of 5-keV Ar^+ ions is focused to a 2-mm spot on the sample. A given time after the ion impact, a ribbon-shaped laser pulse resonantly ionizes a small volume of the desorbed neutrals, thus defining the time of flight (TOF) of the probed species. The ionized particles are then accelerated toward the MCP and are imaged onto the phosphor screen. The image is monitored by the CCD camera and is subsequently stored in the computer. For a single measurement, 30–40 frames, each corresponding to different TOF, are collected and sorted into an intensity map of ejection angles and kinetic energies using a deconvolution procedure described earlier.[8]

III. COMPUTER SIMULATIONS

Molecular-dynamics simulations of the ion-impact event are performed using a 3-keV Ar-ion beam at normal incidence on a Rh{100} microcrystallite containing six layers with about 145 atoms per layer. The interaction between the target atoms is described using the many-body potential constructed based on the Daw-Baskes embedded-atom method (EAM).[15,16] Briefly, in the EAM formalism, the potential energy for the ith atom is given by

$$E_i = F\left[\rho_i = \sum_j \rho_{\text{atomic}}(\mathbf{r}_{ij})\right] + \tfrac{1}{2}\sum_j \varphi(\mathbf{r}_{ij}) , \qquad (1)$$

where $\mathbf{r}_{ij}$ is the distance between atoms i and j. The first term is the embedding function which describes the interaction of the ion core with the electron sea of density ρ_i, and the second term takes the ion-core repulsion into account. The embedding function is a characteristic of a particular atom type and is assumed not to depend on the source of the electron density. Thus, once this function is determined, it may be used in any arbitrary configurations of atoms. It is already shown that the EAM potential developed originally for the Rh{111} surface[11] successfully accounts for the distributions obtained from the Rh{331} stepped surface[17] and from an oxygen-covered Rh{111} surface.[18] Here, the same many-body potential is further used to simulate the desorption process for Rh{100}. To sample a representative area of the surface, 1000 trajectories, each corresponding to a different impact point, are performed over a triangular zone in the center of the crystal which

possesses the irreducible surface symmetry.[19] For this system, the desorption yield of the edge atoms is less than 10% of the total, indicating that the microcrystallite chosen well contains the collision cascades.

IV. RESULTS AND DISCUSSION

The experimental polar-angle (θ) distributions of Rh atoms desorbed from the Rh{100} surface along the $\varphi=0°$ (open) and $\varphi=45°$ (close) azimuthal directions are shown in Fig. 2(b). The off-normal intensity for the 0° azimuth is higher than for the 45° direction, indicating that there is a strong preference for ejection along the open channels of the crystal, a behavior previously observed for Rh{111}.[9] In addition, ejection is focused into a polar angle of about 50° along the open direction and 35° for the close-packed direction.

The results of the classical molecular-dynamics simulation of the desorption process are presented in Fig. 2(b). As can be seen, the measured angular anisotropies are well reproduced by the calculation in the high-kinetic-energy regime. However, the agreement is less satisfactory in the low-energy range (≤ 10 eV). At present, the reason for this discrepancy is not clear. Based on the simulation, about 89% of the desorbed particles originate from the first layer and only 10% from the second layer, indicating that the subsurface atoms make relatively small contributions to the total yield.[20] In Fig. 2(b) the second-layer component of the angular distribution is plotted separately. Similar to the {111} case, an exiting second-layer atom is channeled by the four adjacent surface atoms in the direction normal to the surface [Fig.

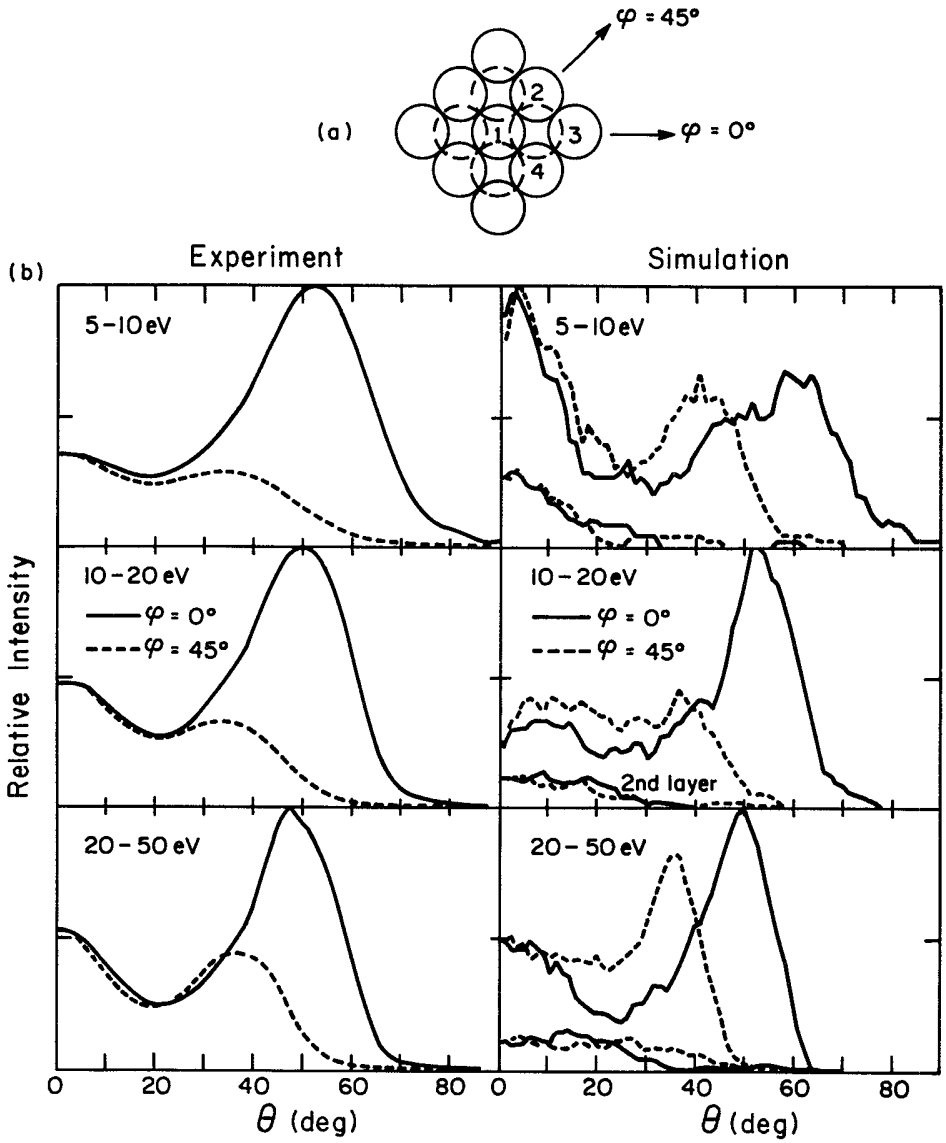

FIG. 2. (a) Rh{100} crystal face with $\varphi=0°$ (open) and $\varphi=45°$ (close) azimuthal directions shown. The dashed circles denote the positions of the second layer atoms. (b) Experimental (right) and calculated (left) polar-angle distributions for Rh atoms desorbed from Rh{100}. Solid lines correspond to ejection along $\varphi=0°$ and the dashed lines along the 45° direction for 5–10 eV (top), 10–20 eV (middle), and 20–50 eV (bottom) energy ranges of the ejected Rh atoms. The curves marked "2nd layer" are the distributions obtained by only collecting the second-layer atoms.

2(a)], contributing to as much as 30% of the yield in this direction.[10,11]

The characteristics of the angular distributions along the two azimuthal directions can be explained by investigating the spatial variation of the potential energy of a surface atom as it leaves the surface. Using the above many-body interaction, the equipotential lines for atom 1 [Fig. 2(a)] ejecting along the $\varphi=0°$ and 45° directions are presented in Fig. 3. The horizontal axis is the atom distance along the surface from its equilibrium position, and the vertical axis denotes its height above the surface. The exact trajectory taken by a particle with a given initial energy and a takeoff angle is rather complicated. However, the following observations help understand the results on a qualitative basis. For $\theta<30°$ the equipotential curves are nearly identical for the two directions considered. As a consequence, in this range of polar angles, the distributions are expected to be very similar, indeed consistent with the experimental observations [Fig. 2(b)]. However, for polar angles greater than 30°, since the nearest-neighbor distance is smaller along the 45° azimuth (Table I), the equipotential lines are more closely spaced. A particle moving in this direction experiences a stronger repulsive force, which tends to bend it more toward the surface normal. Therefore, the peak in the distributions occurs at a smaller angle for ejection along this direction than along $\varphi=0°$, in complete agreement with the measurements.

TABLE I. Interatomic distances for the (100) and (111) faces of a fcc crystal. D_{ij} is the distance between surface atoms i and j [Figs. 2(a) and 4(a)] and D_z is the interplanar separation, both expressed in lattice units ($a_0=3.8$ Å for Rh).

Face	D_{12}	D_{13}	D_{24}	D_z
(100)	0.71	1.00	1.00	0.50
(111)	0.71	1.22	0.71	0.57

Using contour plots of the surface potential energy, the previously published distributions obtained from Rh{111} (Ref. 9) can be understood when compared to the {100} results. This comparison is somewhat simplified due to the fact that the interplanar spacings are roughly the same for these two crystals (Table I). In Fig. 4(b) the angular distributions for the {111} surface are

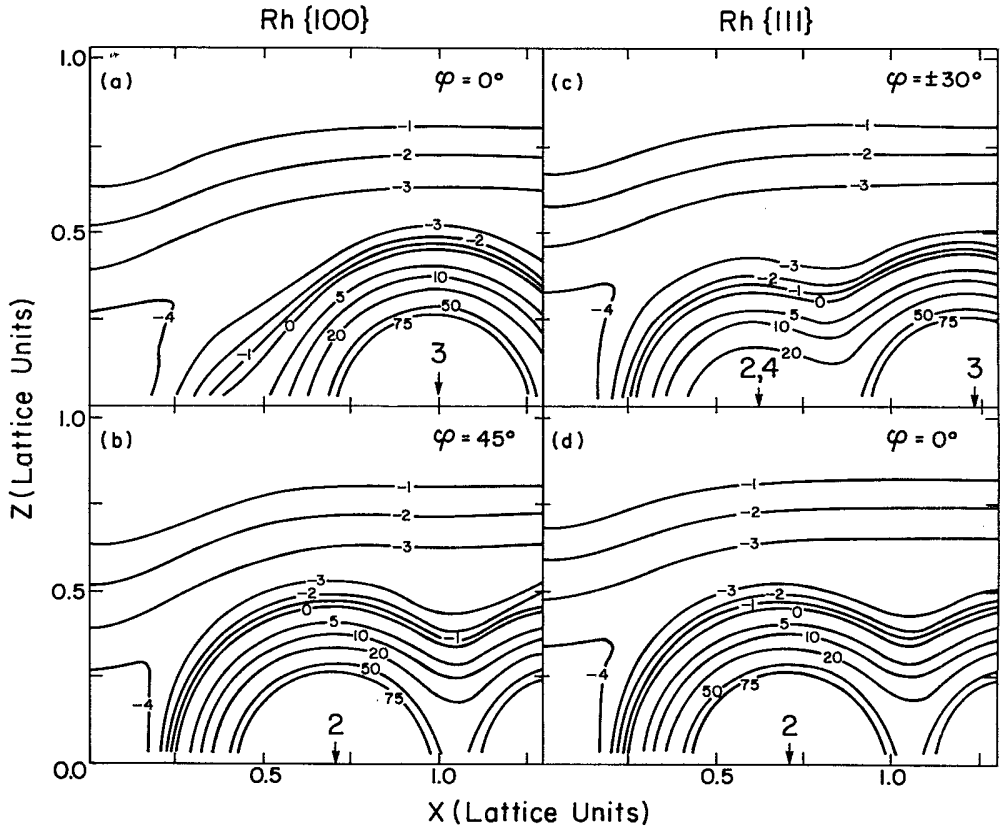

FIG. 3. Contour plots of the potential energy (in eV) of atom 1 desorbing from the Rh{100} surface along (a) $\varphi=0°$ and (b) $\varphi=45°$ [Fig. 2(a)], and from the Rh{111} surface along (c) $\varphi=\pm30°$ and (d) $\varphi=0°$ azimuthal directions [Fig. 4(a)]. The ordinate is the height (in lattice units) above the surface and the abscissa is the atom position (in lattice units) along the surface. The origin corresponds to the equilibrium position of atom 1. The arrows along the horizontal axes denote the nearest-neighbor atoms as they are defined in Figs. 2(a) and 4(a). The arrow labeled "2,4" in (c) corresponds to the projection of the atom 1 and 2 bond length (and the atom 1 and 4 bond length) onto the line connecting atoms 1 and 3. It should be noted that the influence of particles 2 and 4 on ejection along the $\varphi=0°$ of the Rh{100} surface can be seen in (a) at $X\approx0.5$ lattice units. However, since these atoms are farther away on this surface (Table I), the effect is not as prominent. Surface relaxation due to the exiting atom is not taken into account.

presented along $\varphi=+30°$, 0°, and $-30°$ directions, defined in Fig. 4(a). Similar to the {100} results, the intensities are higher along the open directions (i.e., $\varphi=\pm 30°$). Furthermore, the ejection peaks at a polar angle of about 35° along the $\varphi=0°$ and at 40° in the two open directions. The potential-energy contours for an atom leaving the Rh{111} surface are presented in Fig. 3. The equipotential lines for the $\varphi=0°$ ejection are nearly identical to those along the 45° direction of the {100} surface [Fig. 3(b)]. This is basically due to the fact that particles desorbing along these two directions experience very similar local environments. The nearest-neighbor distances (D_{12} in Table I) are identical for these two directions. Moreover, nearby atoms, such as particles 4 and 5 on the {111} surface, are sufficiently far away so as to have minimal influence on the path of particle 1 ejecting in the direction of particle 2 (i.e., $\varphi=0°$). This nearly identical local geometry, in turn, leads to very similar angular distributions, consistent with the experimental results. Contour plots of the surface potential energy along the $\pm 30°$ azimuths are presented in Fig. 3(c). Since in this analysis, the top layer is dominant, these two directions become identical and thus have the same equipotential curves. In contrast to the previous contour maps, there exists an additional repulsive feature between the origin and the nearest-neighbor atom. This structure is caused by particles 2 and 4, which are close enough to the path of the exiting atom 1 to repel it [Fig. 4(a)]. Since, along the $\varphi=\pm 30°$ directions, the nearest-neighbor distance D_{13} is the largest (Table I), in the absence of this feature one would expect the peak in the angular distributions to occur at a larger angle ($\theta>50°$) than along any other direction discussed here. On the contrary, due to the influence of the adjacent atoms 2 and 4, the desorbing particle is deflected more toward the surface normal, leading to a distribution that peaks at a smaller angle than expected otherwise.

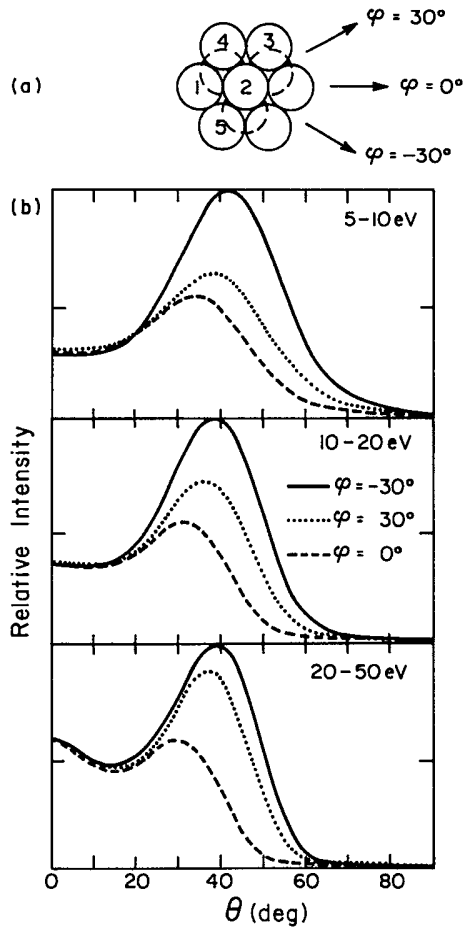

FIG. 4. (a) Rh(111) crystal face with $\varphi=-30°$, 0°, and $+30°$ azimuthal directions shown. The dashed circles denote the positions of the second-layer atoms. (b) Experimental angular distributions for Rh atoms desorbed from Rh{111} (taken from Ref. 9). Solid lines correspond to ejection along $\varphi=-30°$, the dashed lines along $\varphi=0°$, and dotted lines along $\varphi=+30°$ directions for 5–10 eV (top), 10–20 eV (middle), and 20–50 eV (bottom) energy ranges.

This analysis emphasizes the importance of the relative positions of surface atoms. For an open surface such as the {100}, the peak position in the angular distribution correlates with the nearest-neighbor distance. The larger this separation, the larger the peak angle, as is evident when comparing the distribution along $\varphi=0°$ to that for the 45° ejection. On the other hand, for a more closely packed surface such as {111}, the nearest-neighbor distance, alone, is not sufficient to account for all the observations. In this case the influence of other nearby atoms needs to be taken into consideration. When the adjacent particles are far away, as is the case for the $\varphi=0°$ direction, the nearest-neighbor distance is still the determining factor. As a consequence, the distribution along this azimuth is very similar to that for the 45° ejection of the {100} surface. However, for $\varphi=\pm 30°$, even though the nearest-neighbor distance is larger than that along the 0° direction of the {100}, the peak in its angular distribution occurs closer to normal. This is attributed to the fact that, in this case, the nearby atoms are close enough to the path of an exiting particle to deflect it toward the surface normal, leading to a distribution that peaks at a smaller angle than expected based on the nearest-neighbor distance, alone.

Comparison to the Rh{111} results reveals another factor which influences the observed behavior. Even though the surface equipotential curves are identical for the $+30°$ and $-30°$ directions, the angular distributions have very different relative intensities, particularly at low kinetic energies [Fig. 4(b)]. This difference has been attributed to second-layer atoms.[9–11] Briefly, the second-layer registry in the {111} surface is such that, if a second-layer moves towards the surface in the $-30°$ direction, it hits a first-layer atom [Fig. 4(a)]. In other words, there is a second-layer atom that can knock out a first-layer atom in the $-30°$ azimuth but not in the $+30°$ direction. This additional channel, present only along $\varphi=-30°$, leads to an enhancement of the yield in this direction. At higher kinetic energies, however, the ejection is mainly caused by collisions involving the first-layer atoms, and thus an approximate sixfold symmetry is achieved in the distributions. Similarly, on the {100} surface, if a second-layer atom moves toward the surface

along the 0° azimuth, it can knock out a first-layer atom in this direction, a desorption channel not available in the 45° direction [Fig. 2(a)]. Therefore, there are more particles ejected along the $\varphi=0°$ and the ratio of the yield along this direction to that for the 45° ejection decreases as the kinetic energy increases. The latter effect is evident in the experimental results depicted in Fig. 2(b). However, the higher yield along the 0° azimuth is a consequence of this factor as well as the openness of the surface in this direction, an effect discussed previously using the contour maps of the surface potential energy.

Based on the above observations, one can conclude that there are at least two factors important in determining the angular distributions of desorbed atoms from an ion-bombarded single crystal. One is the relative positions of surface atoms, a factor whose influence is clearly demonstrated using the contour plots of the surface potential energy. The second factor is the anisotropy of the momentum imparted to the surface atoms in the last collision. This effect is best illustrated when the influence of the second layer is taken into account.

V. SUMMARY AND CONCLUSIONS

Energy-resolved angular distributions of Rh atoms ejected from an ion-bombarded Rh{100} single crystal have been measured and compared to the previously published results for Rh{111}. Using the same many-body potential developed originally for Rh{111}, good agreement between the experimental results and the classical dynamics calculation of the desorption process has been obtained. By extracting the information available from the molecular-dynamics simulation, we have shown that despite the complexity of the ion-bombardment process, the anisotropies observed in the angular distributions are mainly determined by the extreme local environment surrounding a surface atom. In other words, it is the geometrical structure of the very-near-surface region that controls the angular anisotropies. The registry of the second-layer atoms with respect to the first layer causes the momentum imparted in the last collision to a surface atom to be highly directional. This, in turn, leads to the preferential ejection of the particle along certain crystallographic directions. The exact trajectory taken by the exiting atom is then influenced by the presence of the nearby surface atoms. On an open surface such as {100}, the nearest-neighbor particle exerts the greatest influence. The closer this atom, the more the desorbing particle is deflected towards the surface normal, and hence, the smaller the peak position in the angular distributions. However, for a more closely packed surface such as the {111}, the effect of other nearby atoms needs to be taken into account.

These observations are rather significant in terms of providing a simple and comprehensive picture of the mechanisms leading to the observed distributions. Furthermore, they provide an important framework for future developments of any analytical models of the ion-bombardment process.

ACKNOWLEDGMENTS

We wish to thank Kerry Walzl and Andrea Schmalz for their assistance in the early stages of this work. The financial support of the U.S. Office of Naval Research, the U.S. National Science Foundation, and the IBM Program for the Support of the Materials and Processing Sciences is gratefully acknowledged. One of us (B.J.G.) acknowledges partial support from the Camille and Henry Dreyfus Foundation (New York, NY). The Pennsylvania State University supplied a generous grant of computer time for these studies. One of us (Z.P.) would like to thank Polish Ministry of Sciences Project No. CPBR-01-09 for additional support.

*On leave from Institute of Physics, Jagellonian University, ulica Reymonta 4, PL-30-059 Kraków 16, Poland.

[1]M. T. Robinson, in *Sputtering by Particle Bombardment*, edited by R. Behrisch (Springer-Verlag, Berlin, 1981), p. 73.

[2]G. K. Wehner, J. Appl. Phys. **26**, 1056 (1955).

[3]R. H. Silsbee, J. Appl. Phys. **28**, 1246 (1957).

[4]C. Lehmann and P. Sigmund, Phys. Status Solidi **16**, 507 (1966).

[5]H. H. Andersen, Nucl. Instrum. Methods B **18**, 321 (1987).

[6]D. H. Harrison, Jr., Radiat. Eff. **70**, 1 (1983).

[7]W. Szymczak and K. Wittmaak, in *Proceedings of a Symposium on Sputtering*, edited by P. Varga, G. Betz, and F. P. Viebock (IAEA, Vienna, 1980), p. 236.

[8]P. H. Kobrin, G. A. Schick, J. P. Baxter, and N. Winograd, Rev. Sci. Instrum. **57**, 1354 (1986).

[9]J. Singh, C. T. Reimann, J. P. Baxter, G. A. Schick, P. H. Kobrin, B. J. Garrison, and N. Winograd, J. Vac. Sci. Technol. A **5**, 1191 (1987).

[10]B. J. Garrison, C. T. Reimann, N. Winograd, and D. E. Harrison, Jr., Phys. Rev. B **36**, 3516 (1987).

[11]B. J. Garrison, N. Winograd, D. M. Deaven, C. T. Reimann, D. Y. Lo, T. A. Tombrello, D. E. Harrison, Jr., and M. H. Shapiro, Phys. Rev. B **37**, 7197 (1988).

[12]W. Oed, B. Dötsch, L. Hammer, K. Heinz, and K. Müller, Surf. Sci. **207**, 55 (1988).

[13]G. B. Fisher and S. J. Schmieg, J. Vac. Sci. Technol. A **1**, 1064 (1983).

[14]D. G. Castner, B. A. Sexton, and G. A. Somorjai, Surf. Sci. **71**, 519 (1978).

[15]M. S. Daw and M. I. Baskes, Phys. Rev. Lett. **50**, 1285 (1983).

[16]M. S. Daw and M. I. Baskes, Phys. Rev. B **29**, 6443 (1984).

[17]C. T. Reimann, K. Walzl, M. El-Maazawi, D. M. Deaven, B. J. Garrison, and N. Winograd, J. Chem. Phys. **89**, 2539 (1988).

[18]C. T. Reimann, M. El-Maazawi, K. Walzl, B. J. Garrison, and N. Winograd, J. Chem. Phys. **90**, 2027 (1989).

[19]D. E. Harrison, Jr., N. S. Levy, J. P. Johnson III, and H. M. Effron, J. Appl. Phys. **39**, 3742 (1968).

[20]Based on the simulations, the average yield as defined by the number of ejected atoms per incident ion is ≈ 2 for Rh{100}, in contrast to 3.5 for the more closely packed Rh{111}. Also for Rh{111}, about 93% of the total yield is attributed to the first layer and only 6% to the second layer.